Model for diffusion on deformable lattices. II. Tracer diffusion

T. Ala-Nissila,* J. Kjoll, and S. C. Ying
Department of Physics, Brown University, Providence, Rhode Island 02912

R. A. Tahir-Kheli
Institut Max von Laue-Paul Langevin, Centre de Tri, avenue des Martyrs, Boîte Postale 156X, 38042 Grenoble CEDEX, France
and Department of Physics, Temple University, Philadelphia, Pennsylvania 19122
(Received 26 November 1990)

We present results of theoretical studies of tracer diffusion in a lattice-gas model that has been proposed to explain the anomalous diffusion anisotropy of H adatoms on a W(110) surface. This study complements our previous calculations of collective diffusion within the model (Ala-Nissila *et al.*, preceding paper). We first perform extensive Monte Carlo random-walk simulations of tracer diffusion including only the intracell hard core interactions. We then use the Green's-function method to develop an analytic mean-field theory for the tracer-diffusion coefficients. We also present a derivation of an improved solution to second order in the Green's-function expansion. The range of validity of these analytic results is examined by comparison with the simulations. Finally, we compare the properties of tracer diffusion with collective diffusion.

I. INTRODUCTION

In the case of a single particle performing a random walk on an inert, empty lattice, the corresponding diffusion constant can trivially be written down as Ia^2/z, where z is the coordination number of the lattice, I is the (microscopic) jump rate, and a the lattice constant (i.e., the length of each jump).[1] However, in the presence of other particles, the diffusion process becomes correlated,[2] which usually leads to a difference in the behavior of single particle or tracer diffusion and that of collective or chemical diffusion processes.[3] Namely, even in the case of only single-site hard-core interactions, collective diffusion is independent of coverage,[4] while tracer diffusion shows strong interparticle correlation effects.[2,5] In the preceding paper[6] (hereafter referred to as I), we have presented a detailed study of the properties of collective diffusion in a model of diffusion in a deformable lattice. The model we have studied is a two-step lattice-gas model which was recently introduced[7] to explain the observed anomalous diffusion anisotropy of H adatoms on a W(110) surface.[8,9] The two-step model is characterized by a *branching ratio* $r \equiv M/I$, which is the ratio of intracell-to-intercell diffusion rates M and I, respectively. The existence of an intracell diffusion jump has been postulated on the basis of a hydrogen-induced local distortion of The W(110) surface.[7,8] As a consequence of this, the model includes an additional in-cell hard-core exclusion interaction which makes the collective diffusion nontrivial even without other adatom interactions, as we have shown in I.

In this work we have undertaken a systematic and comprehensive study of tracer diffusion within the lattice-gas model. This complements our previous calculations of collective diffusion.[6,7] Following I, we will concentrate on the case of where the double occupancy of each cell is strictly forbidden. A detailed study of both tracer and collective diffusion in the presence of realistic, finite adatom interactions is planned to be presented in a subsequent publication.[10] Here we begin by presenting results of extensive Monte Carlo random-walk simulations as a function of coverage for various values of r. Then, using the Green's-function method, we obtain an analytic mean-field solution of tracer-diffusion coefficients. To improve upon the mean-field approximation, we present a derivation of a solution to second order in the Green's-function expansion. Both of these analytic solutions are compared with Monte Carlo simulations. Finally, we contrast the behavior of tracer diffusion to collective diffusion in the model and discuss the relevance of our results with respect to the H/W(110) system.

II. MONTE CARLO SIMULATIONS

The surface of the W(110) plane forms a centered rectangular lattice, with adatoms adsorbed on the long bridge sites within the "hourglass" potential of Fig. 1(a) of I. The principal axes of diffusion are along the $(1\bar{1}0)$ and (001) directions, denoted by y and x, respectively. Assuming a locally distorted surface, we have shown within the random-walk picture that the diffusion problem can be described by a lattice-gas model with rates M and I for intracell and intercell diffusion jumps, respectively.[6,7] The branching ratio $r \equiv M/I$ then determines the value of the diffusion anisotropy, which, in the zero coverage limit, is given exactly by[7]

$$\frac{D_{yy}}{D_{xx}} = \frac{r}{r+2}\left[\frac{b}{a}\right]^2 . \tag{2.1}$$

Here a_0 and b_0 denote the dimensions of the underlying

unit cell, and $(b/a)^2=2$ for W(110). As we have shown in I, this simple result gives a reasonably accurate finite-coverage description of the true *collective*-diffusion anisotropy for branching ratios $r \gtrsim 1$, where interparticle correlations are relatively weak. In the limit $r \to \infty$, where the effect of the in-cell exclusion vanishes, (2.1) becomes exact for collective diffusion, and all coverage dependence of D_{yy} and D_{xx} vanishes.[4] However, for *tracer* diffusion, such is no longer the case. We can see this from the well-known results of tracer diffusion for simple, isotropic lattices where the tracer-diffusion coefficient can be written as $D(c)=D_0(1-c)f(c)$, where $D_0(1-c)$ defines the mean-field diffusion coefficient with $D_0 \equiv D(c=0)$, c is the background density (coverage), and $f(c) \leq 1$ is a tracer-correlation factor.[2,5] Thus, in contrast to the *collective*-diffusion case, we expect the corresponding *tracer*-correlation factors for our model to exhibit highly nontrivial behavior for *all* values of r and reduce to the known isotropic lattice results[2,5,11-13] in the limit $r \to \infty$.

To study the properties of tracer diffusion within the lattice-gas model, we have first performed extensive Monte Carlo (MC) random-walk simulations as a function of coverage, for several values of the branching ratio r. Following I, we will concentrate here on the case of intracell hard-core interactions. To obtain D_{yy} and D_{xx}, we have used the definition

$$D_{\alpha\alpha}=\frac{1}{N}\lim_{t\to\infty}\frac{1}{t}\sum_{i=1}^{N}\langle |R_\alpha^i(0)-R_\alpha^i(t)|^2\rangle \ , \quad \alpha=x,y \ , \tag{2.2}$$

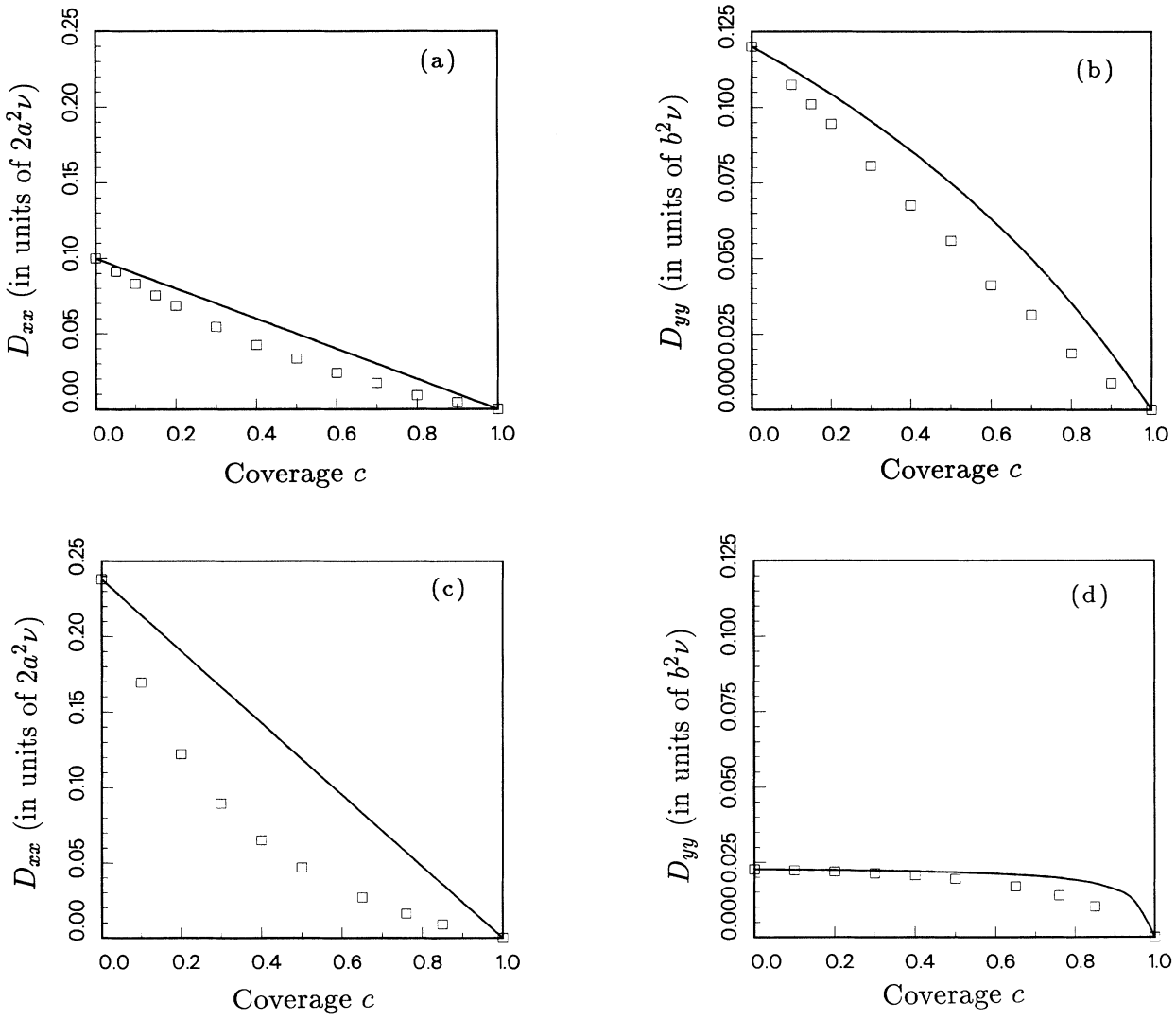

FIG. 1. Tracer-diffusion simulations (open squares) for the geometry of Fig. 3 of paper I, where $2a^2=b^2$. The magnitude of the overall rate constant ν is arbitrary. For comparison, the MF results of Sec. III A are also shown by a solid line. (a) D_{xx} and (b) D_{yy} for $r=3$, (c) D_{xx} and (d) D_{yy} for $r=\frac{1}{10}$. The error bars for MC results are smaller than the size of the points.

where N is the number of particles, $R_\alpha^i(t)$ denotes the spatial component of the position vector of the ith particle at time t, and $\langle\ \rangle$ denotes configuration averaging. In the random-walk algorithm, each diffusing particle is tagged and the displacements are averaged over all of the N particles to improve statistics.

Typically, in the simulations we have used systems of the sizes 30×30, 60×60, and 100×100, with fully periodic boundary conditions. Most of the results presented here are for 60×60 lattices. Depending on the coverage, times up to of 200–5000 MC steps per particle were used in evaluating (2.2). The product of the particle number N and configuration averaging over repeated time intervals was typically of the order of 10^5–10^6. Particular care was taken to ensure that the simulations have reached the proper hydrodynamic limit by performing test runs to very long times. However, in most cases the hydrodynamic limit seemed to set in just after each particle had moved a few lattice spacings on the average. To obtain good accuracy, least-squares fitting was done at various parts of the displacement curves and the final result was chosen to be the average of these fits. In our simulations finite-size effects were very weak, and the logarithmic term present in two dimensions[12,13] was not detectable in the data.

In Fig. 1 we show the results of MC simulations as a function of coverage for $r=3$ and $\frac{1}{10}$, corresponding to the geometry of the W(110) surface. As expected, both D_{yy} and D_{xx} are now monotonically decreasing functions of c, in contrast to the collective diffusion case (cf. Fig. 2 in I). For $r=3$ the qualitative behavior of diffusion is similar to the isotropic lattice limit of $r\to\infty$. However, for $r=\frac{1}{10}$ diffusion in the y direction is strongly suppressed and varies rather slowly as a function of c. To quantitatively unravel this nontrivial coverage dependence of tracer diffusion, in the next section we will develop an analytic theory to calculate D.

III. GREEN'S-FUNCTION METHOD FOR TRACER DIFFUSION AT ALL COVERAGES

To calculate the effect of interparticle correlations to tracer diffusion of noninteracting lattice-gas particles, an equation of motion method based on Green's-function formalism has been developed by Tahir-Kheli and Elliott[11] (TKE) and further refined by Tahir-Kheli and others.[5,12–15] As we have demonstrated in I, the TKE formalism can be easily generalized for our lattice-gas model, where the new feature is the intracell exclusion interaction in addition to the usual single-site hard-core interaction. In this section we will further apply the TKE formalism and develop an analytic theory for the tracer-diffusion case. Although formally somewhat more complicated, this case shares several common features with the derivation of the collective-diffusion theory in I, to which we will frequently refer at the appropriate stages.

The general lattice-gas model we consider is geometrically identical to the collective-diffusion case (Fig. 3 of I). It now consists of a single tracer particle in a sea of background particles. We will consider the most general case where the background particles can be different from the tracer particles, in the sense that their corresponding hopping rates are distinct. The diffusing particles jump between neighboring lattice cells, which have sublattices A and B. Double occupation of a cell by either the tracer and a background particle, or two background particles, is forbidden. We let $p(t)$ be the stochastic occupancy variable of the tracer particle, while $n(t)$ refers to the background particles. If at a time t, a site A in cell g is occupied by the tracer, $p_g^A(t)=1$; otherwise, $p_g^A(t)=0$. Similarly, $n_g^A(t)=1$ or 0, according to whether or not one of the background particles sits on sublattice A in cell g. Using these variables, we can write down the following rate equation for the tracer particle occupying sublattice A at cell g:

$$\frac{d}{dt}p_g^A(t)=-M^{A0}p_g^A(t)+M^{B0}p_g^B(t)-\sum_f p_g^A(t)I^{A0}(gf)[1-n_f^B(t)-n_f^A(t)]+\sum_f p_f^B(t)I^{B0}(fg)[1-n_g^A(t)-n_g^B(t)]\ . \tag{3.1}$$

The corresponding equation for sublattice B follows by interchanging labels for A and B. M^{A0} is the jump rate associated with the tracer particle hopping from A to B within the hourglass, while M^{B0} denotes the rate in the opposite direction. $I^{A0}(gf)$ and $I^{B0}(gf)$ are tracer hopping rates associated with an intercell jump from cell g to cell f. Following I, $I^{A0}(gf)=I^{A0}$ for $\mathbf{f}-\mathbf{g}=\boldsymbol{\delta}_1$ or $\boldsymbol{\delta}_2$, $I^{B0}(fg)=I^{B0}$ for $\mathbf{f}-\mathbf{g}=-\boldsymbol{\delta}_1$ or $-\boldsymbol{\delta}_2$, and both are zero otherwise. Here $\boldsymbol{\delta}_1=(a,b)$ and $\boldsymbol{\delta}_2=(-a,b)$ connect adjacent cells, as shown in Fig. 3 of I.

The background particles are governed by similar equations of motion. Taking into account that a background particle can be blocked by other background particles as well as the tracer, we find

$$\frac{d}{dt}n_g^A(t)=-M^An_g^A(t)+M^Bn_g^B(t)-\sum_f I^A(gf)n_g^A(t)[1-n_f^B(t)-n_f^A(t)-p_f^B(t)-p_f^A(t)]+\sum_f I^B(fg)n_f^B(t)[1-n_g^A(t)-n_g^B(t)-p_g^A(t)-p_g^B(t)]\ , \tag{3.2}$$

for a background particle on sublattice A in cell g. Again, the corresponding equation for sublattice B follows trivially. The hopping rates M^A, M^B, I^A, and I^B of the background particles correspond to M^{A0}, M^{B0}, I^{A0}, and I^{B0} in (3.1), but they need not be identical. However, the detailed balance condition must be obeyed by both the tracer particle and background particles.

The background occupancy variables can be written in terms of fluctuations $u_g^S(t)\equiv n_g^S(t)-c^S$ on sublattice $S=A$ or

B. The components of the tracer-diffusion tensor can be extracted from the pole of the retarded Green's function for the tracer:

$$G^{S}_{gg'}(t)=-2\pi i\Theta(t)\langle p^{S}_{g}(t)p^{A}_{g'}(0)\rangle \ , \tag{3.3}$$

where $\Theta(t)$ is the Heaviside step function and the angular brackets denote a statistical average. The corresponding four next-higher-order Green's functions are given by

$$G^{SS'}_{glg'}=\langle\langle p^{S}_{g}(t)u^{S'}_{l}(t);p^{A}_{g'}(0)\rangle\rangle \ , \tag{3.4}$$

for $S,S'=A$ or B. To obtain an equation of motion for $G^{S}_{gg'}(t)$, we make use of the corresponding rate equation (3.1). The equal-time term from the derivative of the step function is given by

$$\begin{aligned}-2\pi i\delta(t)\langle p^{S}_{g}(t)p^{A}_{g'}(0)\rangle &=-2\pi i\delta(t)\langle p^{A}_{g}(0)\rangle\delta_{gg'}\delta_{S,A}\\ &=-2\pi i\delta(t)\frac{1}{N}\delta_{gg'}\delta_{S,A} \ ,\end{aligned}$$

where N is the total number of lattice sites. Using the double Fourier transforms defined in I, we can write the corresponding equations of motion for $G^{A}_{\mathbf{k}}(\omega)$ and $G^{B}_{\mathbf{k}}(\omega)$ in reciprocal and frequency space as

$$\begin{aligned}[-i\omega+M^{A0}+vJ^{A0}(0)]G^{A}_{\mathbf{k}}(\omega)-[M^{B0}+vJ^{B0}(-\mathbf{k})]G^{B}_{\mathbf{k}}(\omega)=&-\frac{i}{N}+I^{A0}\sum_{\delta}\frac{1}{N}\sum_{\mu}[e^{i\mu\cdot\delta}G^{AA}_{\mathbf{k}-\mu,\mu}(\omega)+e^{i\mu\cdot\delta}G^{AB}_{\mathbf{k}-\mu,\mu}(\omega)]\\ &-I^{B0}\sum_{\delta}\frac{1}{N}\sum_{\mu}e^{i\mathbf{k}\cdot\delta}[e^{-i\mu\cdot\delta}G^{BB}_{\mathbf{k}-\mu,\mu}(\omega)+e^{-i\mu\cdot\delta}G^{BA}_{\mathbf{k}-\mu,\mu}(\omega)]\end{aligned} \tag{3.5}$$

and

$$\begin{aligned}&[-i\omega+M^{B0}+vJ^{B0}(0)]G^{B}_{\mathbf{k}}(\omega)-[M^{A0}+vJ^{A0}(-\mathbf{k})]G^{A}_{\mathbf{k}}(\omega)\\ &\quad=-I^{B0}\sum_{\delta}\frac{1}{N}\sum_{\mu}[e^{-i\mu\cdot\delta}G^{BB}_{\mathbf{k}-\mu,\mu}(\omega)+e^{-i\mu\cdot\delta}G^{BA}_{\mathbf{k}-\mu,\mu}(\omega)]-I^{A0}\sum_{\delta}\frac{1}{N}\sum_{\mu}e^{-i\mathbf{k}\cdot\delta}[e^{i\mu\cdot\delta}G^{AA}_{\mathbf{k}-\mu,\mu}(\omega)+e^{i\mu\cdot\delta}G^{AB}_{\mathbf{k}-\mu,\mu}(\omega)] \ .\end{aligned} \tag{3.6}$$

Here μ is summed over the first Brillouin zone, δ is summed over δ_1 and δ_2, and the vacancy factor $v\equiv(1-c)\equiv(1-c^{A}-c^{B})$. The quantity $J^{S0}(0)\equiv\sum_{f}I^{S0}(gf)$ and

$$\begin{aligned}J^{A0}(\mathbf{k})&=\sum_{\mathbf{g}-\mathbf{f}}I^{A0}(gf)e^{-i\mathbf{k}\cdot(\mathbf{g}-\mathbf{f})}\\ &=I^{A0}(e^{i\mathbf{k}\cdot\delta_1}+e^{i\mathbf{k}\cdot\delta_2}) \ .\end{aligned}$$

Similarly, $J^{B0}(\mathbf{k})=I^{B0}(e^{-i\mathbf{k}\cdot\delta_1}+e^{-i\mathbf{k}\cdot\delta_2})$. We also note that the detailed balance conditions needed to derive (3.5) and (3.6) are

$$M^{A0}I^{B0}=M^{B0}I^{A0} \ , \tag{3.7}$$

for the tracer particle rates, stand identical to those given in I for the background particles, i.e., $c^{A}M^{A}=c^{B}M^{B}$ and $c^{A}J^{A}(0)=c^{B}J^{B}(0)$.

To solve for the tracer-diffusion tensor, we proceed formally in the same way as in I. To this end we must derive additional equations of motion for the second-order Green's functions in (3.4). However, we will first present the mean-field theory for the tracer-diffusion case.

A. Mean-field solution

Within the mean-field (MF) approximation, we neglect all second-order Green's functions in (3.5) and (3.6), which, in addition to the tracer occupancy variable, also involve a density-fluctuation field for the background particles. This leads to the set of equations

$$\begin{bmatrix}[-i\omega+M^{A0}+vJ^{A0}(0)] & -[M^{B0}+vJ^{B0}(-\mathbf{k})]\\ -[M^{A0}+vJ^{A0}(-\mathbf{k})] & [-i\omega+M^{B0}+vJ^{B0}(0)]\end{bmatrix}\begin{bmatrix}G^{A}_{\mathbf{k}}(\omega)\\ G^{B}_{\mathbf{k}}(\omega)\end{bmatrix}=\begin{bmatrix}-i/N\\ 0\end{bmatrix} \ . \tag{3.8}$$

We observe that the background particles enter only through the vacancy factor v in (3.8). We can obtain the elements of the diffusion tensor from the fact that the diffusive pole of the Green's functions occurs at $\omega=-i\mathbf{k}\cdot\mathsf{D}\cdot\mathbf{k}$ in the limit $\mathbf{k}\to 0$, $\omega\to 0$. The result is

$$D_{xx}=\frac{2vI^{B0}(M^{A0}+2vI^{A0})}{M^{A0}+M^{B0}+2v(I^{A0}+I^{B0})}a^2 \tag{3.9}$$

and

$$D_{yy}=\frac{2vM^{A0}I^{B0}}{M^{A0}+M^{B0}+2v(I^{A0}+I^{B0})}b^2 . \tag{3.10}$$

To make the connection to our original model of diffusion of identical particles, we set $M^{A0}=M^{B0}=M^0$, $I^{A0}=I^{B0}=I^0$, and $c^A=c^B=c/2$, which gives

$$D_{xx}=vI^0a^2 \tag{3.11}$$

and

$$D_{yy}=\frac{vI^0M^0}{(M^0+2vI^0)}b^2 . \tag{3.12}$$

For the diffusion anisotropy we then obtain, in terms of the branching ratio $r=M^0/I^0$,

$$\frac{D_{yy}}{D_{xx}}=\frac{r}{r+2v}\left[\frac{b}{a}\right]^2 . \tag{3.13}$$

Although (3.13) exactly coincides with the result we obtained for the collective-diffusion case in I, both D_{xx} and D_{yy} differ from their collective counterparts by an additional multiplicative factor v. Interestingly enough, this latter result applies for the isotropic lattice cases as well, where collective diffusion is constant for all coverages $c<1$ and is given simply by $D_0=D(c=0)$[4], as we mentioned in Sec. II . As in I, our results correctly reproduce the simple zero-coverage limit of an independent random walker. It is also interesting to note that while the coverage dependence of D_{xx} in (3.11) is identical to the usual isotropic MF result with $D_0\equiv I^0a^2$, D_{yy} reduces to this simple functional form only in the limit $r\to\infty$.

In Fig. 2 we show results of comparisons of the MF theory with the MC simulations. For the x direction the coverage dependence of D_{xx} is given by a straight line and the MC results lie below this line. For $r=\frac{1}{10}$ the discrepancy between the two results becomes quite large. However, for D_{yy} the unusual form of coverage dependence in (3.12) yields a better agreement for very small values of r, where diffusion in the y direction has a rather weak coverage dependence. This result may be explained as follows. Namely, for small r and low coverages, the rate of motion of the tracer and background particles within the cells becomes very small, while background particles can still move relatively fast in the x direction. This fast motion may cause the correlations of the tracer particle to the background density-fluctuation field to weaken, which would improve the MF approximation. A similar effect in the case of a square lattice with fast background particles has been originally pointed out by Tahir-Kheli.[12] We also note that f_y for the case of collective diffusion exhibits similar behavior in I. However, for large enough coverages the correlations can no longer be ignored. Thus, to improve upon the MF solution, in the next section we will present a derivation of an enhanced solution to second order in the Green's-function expansion.

B. Second-order solution

The mean-field approximation can be systematically improved by including higher-order Green's functions in the equations of motion (3.5) and (3.6). In this section we will follow I and derive second-order corrections, which are obtained from the equations of motion for the Green's functions $G^{SS'}_{glg'}(t)$. We get

$$\begin{aligned}\frac{d}{dt}G^{SS'}_{glg'}(t)=&-2\pi\delta(t)\langle p_g^S(0)u_l^{S'}(0)p_{g'}^A(0)\rangle\\&+\left\langle\!\!\left\langle\left[\frac{d}{dt}p_g^S(t)\right]u_l^{S'}(t);p_{g'}^A(0)\right\rangle\!\!\right\rangle\\&+\left\langle\!\!\left\langle p_g^S(t)\left[\frac{d}{dt}u_l^{S'}(t)\right];p_{g'}^A(0)\right\rangle\!\!\right\rangle ,\end{aligned} \tag{3.14}$$

where the different combinations of SS' give a set of four equations. In the absence of static spatial ordering, the first term on the right-hand side of (3.14) vanishes. However, it is important to note that when $g=l$, variables p_g and u_l can be contracted and $G_{glg'}$ becomes proportional to the Green's function $G_{gg'}$. We also note that terms proportional to $\langle\langle p_g(t)u_l(t)u_{l'}(t);p_{g'}^A(0)\rangle\rangle$ are neglected only if $g\neq l\neq l'$; otherwise, they are contracted.

From (3.14), we proceed exactly as in I by inserting the previous equations of motion and transforming to the Fourier space. Correspondingly, for the second-order Green's functions, we recover a matrix equation which is formally identical to that for collective-diffusion case:

$$\underline{C}\cdot\underline{G}^{(2)}_{\mathbf{k}-\mu,\mu}=\underline{F}\cdot\underline{G}^{(1)}_{\mathbf{k}}+\underline{R}\cdot\underline{\rho}_{\mathbf{k}} . \tag{3.15}$$

The matrix elements of $\underline{C}$, $\underline{F}$, and $\underline{R}$ are, of course, different from I and can be found in the Appendix. In Eq. (3.15),

$$\underline{G}^{(2)}_{\mathbf{k}-\mu,\mu}\equiv\begin{bmatrix}G^{AA}_{\mathbf{k}-\mu,\mu}\\G^{BB}_{\mathbf{k}-\mu,\mu}\\G^{AB}_{\mathbf{k}-\mu,\mu}\\G^{BA}_{\mathbf{k}-\mu,\mu}\end{bmatrix} \tag{3.16}$$

and

$$\underline{G}^{(1)}_{\mathbf{k}}\equiv\begin{bmatrix}G^{A}_{\mathbf{k}}\\G^{B}_{\mathbf{k}}\end{bmatrix} . \tag{3.17}$$

The vector $\underline{\rho}_{\mathbf{k}}$ is given by

$$\underline{\rho}_{\mathbf{k}}=\begin{bmatrix}\rho_1\\\vdots\\\rho_{16}\end{bmatrix} , \tag{3.18}$$

with components ρ_1–ρ_{16}:

$$\rho_1=\rho_{\mathbf{k}}^{AB}(\delta_1)\ ,\quad \rho_2=\rho_{\mathbf{k}}^{AB}(\delta_2)\ ,$$
$$\rho_3=\rho_{\mathbf{k}}^{BA}(-\delta_1)\ ,\quad \rho_4=\rho_{\mathbf{k}}^{BA}(-\delta_2)\ ,$$
$$\rho_5=\rho_{\mathbf{k}}^{AA}(\delta_1)\ ,\quad \rho_6=\rho_{\mathbf{k}}^{AA}(\delta_2)\ ,$$
$$\rho_7=\rho_{\mathbf{k}}^{BB}(-\delta_1)\ ,\quad \rho_8=\rho_{\mathbf{k}}^{BB}(-\delta_2)\ ,$$
$$\rho_9=\rho_{\mathbf{k}}^{AA}(-\delta_1)\ ,\quad \rho_{10}=\rho_{\mathbf{k}}^{AA}(-\delta_2)\ ,$$
$$\rho_{11}=\rho_{\mathbf{k}}^{BB}(\delta_1)\ ,\quad \rho_{12}=\rho_{\mathbf{k}}^{BB}(\delta_2)\ ,$$
$$\rho_{13}=\rho_{\mathbf{k}}^{AB}(-\delta_1)\ ,\quad \rho_{14}=\rho_{\mathbf{k}}^{AB}(-\delta_2)\ ,$$
$$\rho_{15}=\rho_{\mathbf{k}}^{BA}(\delta_1)\ ,\quad \rho_{16}=\rho_{\mathbf{k}}^{BA}(\delta_2)\ . \tag{3.19}$$

Following I, we have defined

$$\rho_{\mathbf{k}}^{SS'}(\delta)\equiv\frac{1}{N}\sum_{\mu} e^{i\mu\cdot\delta}G_{\mathbf{k}-\mu,\mu}^{SS'}(\omega)\ , \tag{3.20}$$

where the sum over μ goes over the first Brillouin zone, and δ is either δ_1 or δ_2.

To solve for the second-order equations of motion in (3.15), we follow the procedures outlined in I. In the fully symmetric case $I^{A0}=I^{B0}=I^0$, $M^{A0}=M^{B0}=M^0$, and $c^A=c^B=c/2$, we obtain

$$D_{xx}=vI^0a^2f_x \tag{3.21}$$

and

$$D_{yy}=\frac{vI^0M^0}{M^0+2vI^0}b^2f_y\ , \tag{3.22}$$

where the *tracer-correlation factors* f_x and f_y represent corrections to the previous MF results (3.11) and (3.12). The diffusion anisotropy can then be written as a function of r as

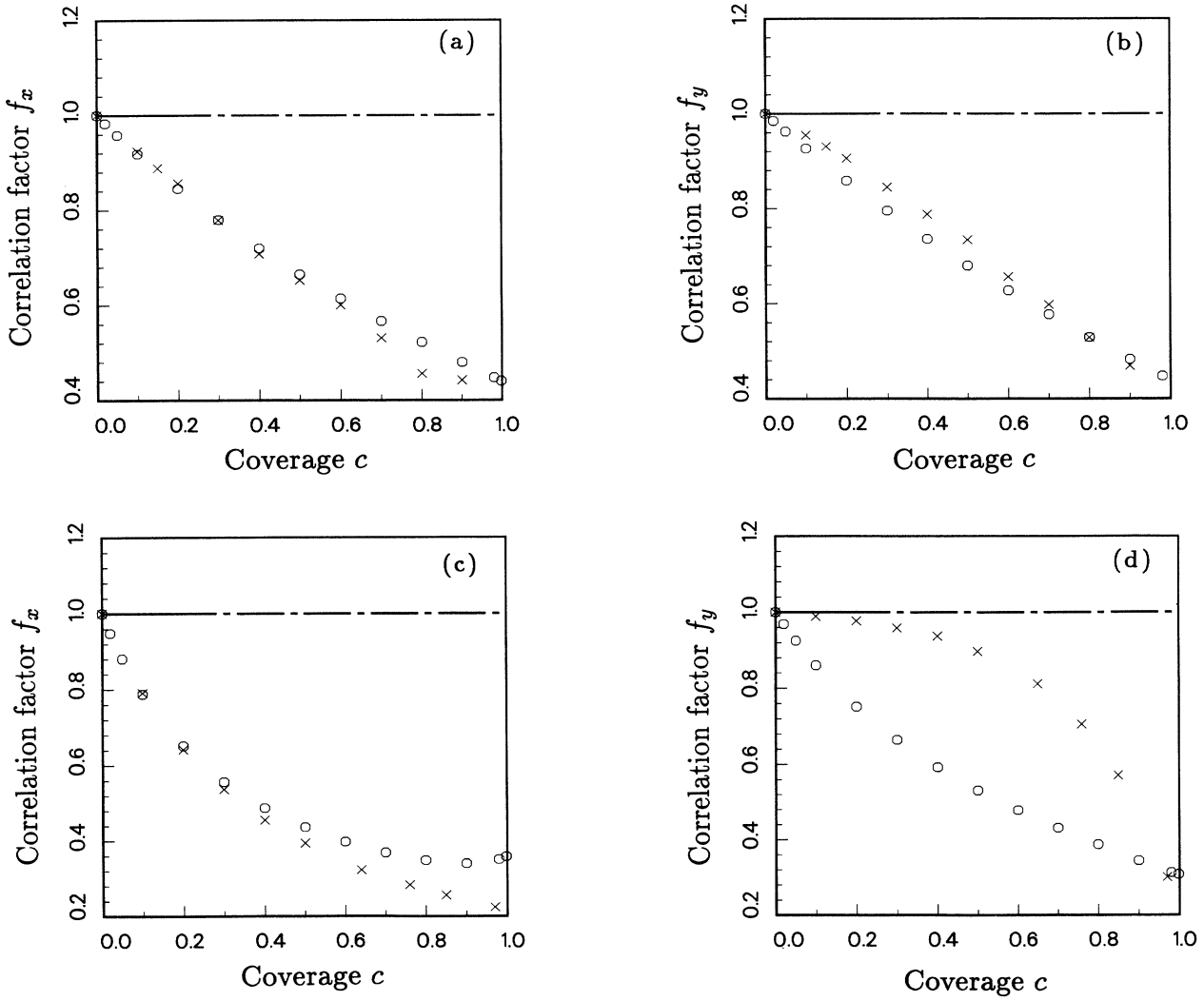

FIG. 2. Comparisons of results for the correlation factors f_x and f_y from the second-order solution of Sec. III B (circles) with MC simulations (crosses). In each case the MF result $f_x\equiv f_y\equiv 1$ is shown for reference by a horizontal dashed line. (a) f_x and (b) f_y for branching ratio $r=3$, (c) f_x and (d) f_y for $r=\frac{1}{10}$. Error bars in the MC results are smaller than or about the size of the crosses.

$$\frac{D_{yy}}{D_{xx}} = \frac{r}{r+2v}\left[\frac{b}{a}\right]^2 \frac{f_y}{f_x} \,. \tag{3.23}$$

These results (3.21) and (3.22) are again formally identical to the collective-diffusion case multiplied by the vacancy factor v; however, the behavior of the tracer-correlation functions is quite different from the collective case, as we will show below.

The numerical integrals over μ were calculated using a 20×20 grid of Gaussian points, which was enough to guarantee convergence. To verify the correctness of our theory, we first computed the correlation functions in the limit of a very large branching ratio $r \gg 1$. As expected, f_y and f_x become identical and the theory in this limit is similar to previous results of Tahir-Kheli and Elliott.[11] Also, in the limit $c \to 0$, we find that the correlation functions correctly approach unity. In Fig. 2 we present results of calculations for the correlation factors in the cases $r=3$ and $\frac{1}{10}$. In each case the MF results are given for comparison by straight horizontal lines. For large values of r, the second-order solution gives a much better agreement with the simulations than the MF theory, as expected. However, as $r \lesssim 1$, for f_x the theory starts to deviate from MC results at large coverages. More dramatically, for f_y the deviation becomes large already for small coverages where the second-order solution shows an overall downward curvature, while the MC results approach mean-field-like behavior for small coverages. Similarly to the collective-diffusion case, the second-order solution does not seem to converge to the correct limit as $c \to 1$, which again is due to terms proportional to $(1-c^A)$ and $(1-c^B)$ present in the neglected higher-order correlation functions.

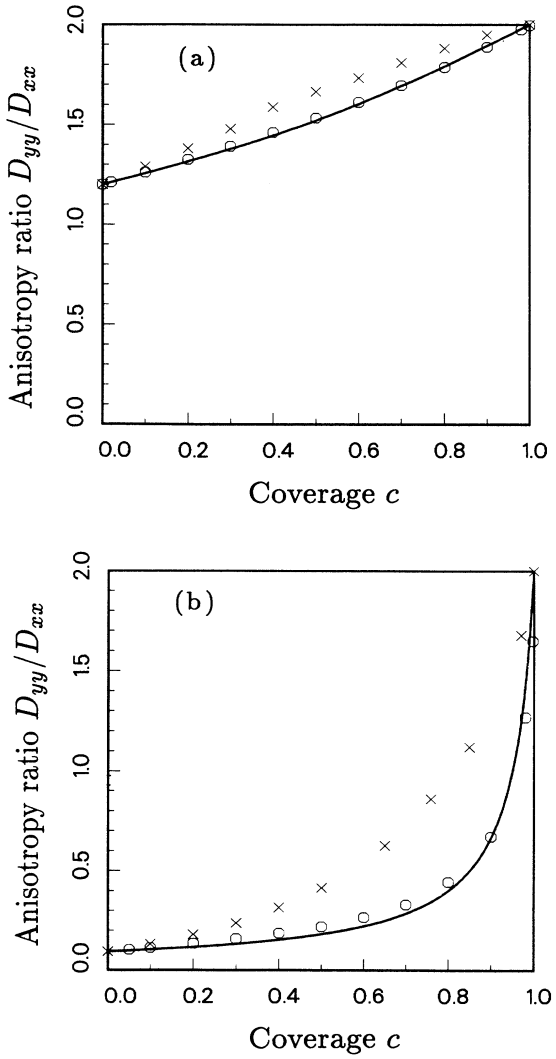

FIG. 3. Anisotropy ratio D_{yy}/D_{xx} for (a) $r=3$ and (b) $r=\frac{1}{10}$ corresponding to the geometry of the W(110) surface in Fig. 3 of paper I. Solid line denotes the MF result (3.23), while crosses denote MC simulations and open circles the analytic second-order solution.

Finally, in Fig. 3 we present results for the anisotropy ratio D_{yy}/D_{xx} for the two branching ratios studied here. Even for $r=3$, the ratio is not described by the analytic theory as accurately as in the case of collective diffusion (see Fig. 5 in I), and the discrepancy as compared to MC results becomes quite large for $r=\frac{1}{10}$. For the latter case, the inaccuracy of the correlation factors within the second-order approximation is reflected in the anisotropy, which is well below its correct value of 2 at $c \to 1$.

IV. SUMMARY AND CONCLUSIONS

In this work we have presented a detailed theoretical study of tracer diffusion in the two-step lattice-gas model with single-site and intracell hard-core interactions. This work complements our preceding paper on collective diffusion in the model. We have first presented accurate MC simulations, which reveal the presence of unusual correlations in the diffusion process of a tracer particle in the sea of identical background particles. To better understand these correlations, we have used the Green's-function method of Tahir-Kheli and Elliott[11] to analytically compute the elements of the tracer-diffusion tensor for the model. Following our previous work, we have first obtained an analytic solution for D within the mean-field approximation. Remarkably enough, these results are formally identical to the collective-diffusion case except for a multiplication by the vacancy factor v. We have also derived an improved solution to second order in the Green's-function expansion, which leads to an expression for D in terms of the MF result multiplied by the corresponding tracer-correlation factors. Our calculations indicate that the interparticle correlations for the tracer-diffusion case are more pronounced than for the collective case. Correspondingly, the second-order solution derived for both cases becomes less accurate for the tracer-diffusion process as r diminishes. However, although the coverage dependence of D for tracer and collective diffusion is very different, the *anisotropy ratio* D_{yy}/D_{xx} behaves in a very similar fashion, at least for the physically interesting cases of branching ratios $r \gtrsim 1$. This is evidenced by a comparison of Fig. 3 with Fig. 5 of I, both of which show D_{yy}/D_{xx} for $r=3$ and $\frac{1}{10}$ for the two modes of diffusion. Although the Green's-function

theory is again quantitatively less accurate than in I, even the MF result (3.13) describes the overall coverage dependence of the ratio correctly in the limit $c \to 0$ and $c \to 1$. Finally, we would like to mention that it may be possible to considerably improve the analytic theory presented here by a self-consistent renormalization of the second-order solution.[13–15] However, this is outside the scope of the present work.

Our results for the diffusion anisotropy of collective diffusion in I have shown that the experimentally observed anomalous anisotropy ratio of about 1.2 of the H/W(110) systems[8] can be qualitatively explained by the symmetry breaking of the cell and the two-step model studied here. At high temperatures and coverage less than $c \lesssim 0.5$, where no phases with long-range order are present in the system,[16] we then expect a relatively weak coverage dependence in the anisotropy ratio of collective diffusion, which result is corroborated by the experiments.[8] The additional results presented in this work indicate that this anisotropy is a *universal* property of the underlying lattice for branching ratios $r \gtrsim 1$. However, for $r = \frac{1}{10}$ our results indicate that D_{yy}/D_{xx} for tracer diffusion is overall somewhat larger than for the collective case. Obviously, it would be very interesting to extend the experimental studies of surface diffusion[17] to include the coverage dependence of tracer diffusion in anisotropic systems such as the W(110) to study the range of validity of such universal behavior.

ACKNOWLEDGMENTS

T.A-N., J.K., and S.C.Y. are supported by an ONR contract. They also want to acknowledge the Illinois National Center for Supercomputing Applications for allocation of computer time in the Cray X-MP. R.A.T-K. thanks Institute Laue-Langevin for hospitality and support during the period this work was carried out.

APPENDIX

This appendix contains expressions for the elements within the matrix equation (3.15). First, the elements of the (4×4) matrix $\underline{C}$ are given by

$$
\begin{aligned}
C_{1,1} &= [-i\omega + \nu^{A0} + \nu^{A} + c^{B}J^{B}(0) - c^{A}J^{A}(\boldsymbol{\mu})] ,\\
C_{1,2} &= 0 ,\\
C_{1,3} &= -[\nu^{B}(\boldsymbol{\mu}) + c^{A}J^{A}(\boldsymbol{\mu}) - c^{B}J^{B}(0)] ,\\
C_{1,4} &= -\nu^{B0}(\mathbf{k}-\boldsymbol{\mu}) ,\\
C_{2,1} &= 0 ,\\
C_{2,2} &= [-i\omega + \nu^{B0} + \nu^{B} + c^{A}J^{A}(0) - c^{B}J^{B}(\boldsymbol{\mu})] ,\\
C_{2,3} &= -\nu^{A0}(\mathbf{k}-\boldsymbol{\mu}) ,\\
C_{2,4} &= -[\nu^{A}(\boldsymbol{\mu}) + c^{B}J^{B}(\boldsymbol{\mu}) - c^{A}J^{A}(0)] ,\\
C_{3,1} &= -[\nu^{A}(\boldsymbol{\mu}) + c^{B}J^{B}(\boldsymbol{\mu}) - c^{A}J^{A}(0)] ,\\
C_{3,2} &= -\nu^{B0}(\mathbf{k}-\boldsymbol{\mu}) ,\\
C_{3,3} &= [-i\omega + \nu^{A0} + \nu^{B} + c^{A}J^{A}(0) - c^{B}J^{B}(\boldsymbol{\mu})] ,\\
C_{3,4} &= 0 ,\\
C_{4,1} &= -\nu^{A0}(\mathbf{k}-\boldsymbol{\mu}) ,\\
C_{4,2} &= -[\nu^{B}(\boldsymbol{\mu}) + c^{A}J^{A}(\boldsymbol{\mu}) - c^{B}J^{B}(0)] ,\\
C_{4,3} &= 0 ,\\
C_{4,4} &= [-i\omega + \nu^{B0} + \nu^{A} + c^{B}J^{B}(0) - c^{A}J^{A}(\boldsymbol{\mu})] ,
\end{aligned}
\tag{A1}
$$

where we have defined $\nu^{S} \equiv M^{S} + vJ^{S}(0)$ and $\nu^{S}(\mathbf{k}) \equiv M^{S} + vJ^{S}(-\mathbf{k})$ for all sublattice indices S.

The (4×2) matrix $\underline{F}$ has elements

$$
\begin{aligned}
F_{1,1} &= c^{A}[i\omega - \nu^{A0} + J^{A}(\boldsymbol{\mu}) + vJ^{A0}(-\boldsymbol{\mu})] - c^{B}J^{B}(0) ,\\
F_{1,2} &= c^{A}M^{B0} ,\\
F_{2,1} &= c^{B}M^{A0} ,\\
F_{2,2} &= c^{B}[i\omega - \nu^{B0} + J^{B}(\boldsymbol{\mu}) + vJ^{B0}(-\boldsymbol{\mu})] - c^{A}J^{A}(0) ,\\
F_{3,1} &= c^{B}[i\omega - \nu^{A0} + J^{B}(\boldsymbol{\mu}) + vJ^{A0}(-\boldsymbol{\mu})] - c^{A}J^{A}(0) ,\\
F_{3,2} &= c^{B}M^{B0} ,\\
F_{4,1} &= c^{A}M^{A0} ,\\
F_{4,2} &= c^{A}[i\omega - \nu^{B0} + J^{A}(\boldsymbol{\mu}) + vJ^{B0}(-\boldsymbol{\mu})] - c^{B}J^{B}(0) .
\end{aligned}
\tag{A2}
$$

For the (4×16) matrix $\underline{R}$, all elements appear in pairs. The elements $R_{i,2j}$ $(i=1,2,3,4;\ j=1,2,3,\ldots,8)$ follow from the preceding elements $R_{i,2j-1}$ by letting $\boldsymbol{\delta}_1 \to \boldsymbol{\delta}_2$. Below, this is shown for the pair $R_{1,1}$ and $R_{1,2}$:

$$
\begin{aligned}
R_{1,1} &= -c^{A}I^{A0}e^{-i\boldsymbol{\mu}\cdot\boldsymbol{\delta}_1} - c^{A}I^{A} - vI^{B} ,\\
R_{1,2} &= R_{1,1}(\boldsymbol{\delta}_1 \to \boldsymbol{\delta}_2) ,\\
R_{1,3} &= c^{A}I^{B0}e^{i\mathbf{k}\cdot\boldsymbol{\delta}_1}e^{-i\boldsymbol{\mu}\cdot\boldsymbol{\delta}_1} - vI^{B0}e^{i\mathbf{k}\cdot\boldsymbol{\delta}_1} ,\\
R_{1,5} &= -c^{A}I^{A} + (v - c^{A})I^{A0}e^{-i\boldsymbol{\mu}\cdot\boldsymbol{\delta}_1} ,\\
R_{1,7} &= c^{A}I^{B0}e^{i\mathbf{k}\cdot\boldsymbol{\delta}_1}e^{-i\boldsymbol{\mu}\cdot\boldsymbol{\delta}_1} ,\\
R_{1,9} &= (c^{B}I^{B} + vI^{A})e^{i\boldsymbol{\mu}\cdot\boldsymbol{\delta}_1} ,\\
R_{1,11} &= 0 ,\\
R_{1,13} &= c^{B}I^{B}e^{i\boldsymbol{\mu}\cdot\boldsymbol{\delta}_1} ,\\
R_{1,15} &= 0 ,\\
R_{1,16} &= 0 ,\\
R_{2,1} &= c^{B}I^{A0}e^{i(\boldsymbol{\mu}-\mathbf{k})\cdot\boldsymbol{\delta}_1} - vI^{A0}e^{-i\mathbf{k}\cdot\boldsymbol{\delta}_1} ,\\
R_{2,3} &= -c^{B}I^{B0}e^{i\boldsymbol{\mu}\cdot\boldsymbol{\delta}_1} - c^{B}I^{B} - vI^{A} ,\\
R_{2,5} &= c^{B}I^{A0}e^{i(\boldsymbol{\mu}-\mathbf{k})\cdot\boldsymbol{\delta}_1} ,
\end{aligned}
$$

$$
\begin{aligned}
R_{2,7} &= -c^B I^B + (v - c^B) I^{B0} e^{-i\mu\cdot\delta_1} , \\
R_{2,9} &= 0 , \\
R_{2,11} &= (c^A I^A + v I^B) e^{-i\mu\cdot\delta_1} , \\
R_{2,13} &= 0 , \\
R_{2,15} &= c^A I^A e^{-i\mu\cdot\delta_1} , \\
R_{3,1} &= [(v - c^B) I^{A0} + c^A I^A + v I^B] e^{-i\mathbf{k}\cdot\delta_1} , \\
R_{3,3} &= c^B I^{B0} e^{-i(\mu-\mathbf{k})\cdot\delta_1} , \\
R_{3,5} &= (c^A I^A - c^B I^{A0}) e^{-i\mathbf{k}\cdot\delta_1} , \\
R_{3,7} &= (-v I^{B0} + c^B I^{B0} e^{-i\mu\cdot\delta_1}) e^{i\mathbf{k}\cdot\delta_1} , \\
R_{3,9} &= -(v I^A + c^B I^B) , \\
R_{3,11} &= 0 , \\
R_{3,13} &= -c^B I^B , \\
R_{3,15} &= 0 , \\
R_{4,1} &= c^A I^{A0} e^{i(\mu-\mathbf{k})\cdot\delta_1} , \\
R_{4,3} &= [(v - c^A) I^{B0} + c^B I^B + v I^A] e^{i\mathbf{k}\cdot\delta_1} , \\
R_{4,5} &= -v I^{A0} e^{i\mathbf{k}\cdot\delta_1} + c^A I^{A0} e^{i(\mu-\mathbf{k})\cdot\delta_1} , \\
R_{4,7} &= (c^B I^B - c^A I^{B0}) e^{i\mathbf{k}\cdot\delta_1} , \\
R_{4,9} &= 0 , \\
R_{4,11} &= -(v I^B + c^A I^A) , \\
R_{4,13} &= 0 , \\
R_{4,15} &= -c^A I^A .
\end{aligned}
\tag{A3}
$$

---

*Permanent address: Department of Physics, Tampere University of Technology, P.O. Box 527, SF-33101 Tampere, Finland.

[1]See, e.g., K.W. Kehr, R. Kutner, and K. Binder, Phys. Rev. B **23**, 4391 (1981).

[2]K. W. Kehr and K. Binder, in *Applications of the Monte Carlo Method in Statistical Physics,* edited by K. Binder (Springer-Verlag, New York, 1987), and references cited therein.

[3]G. Mazenko, J. R. Banavar, and R. Gomer, Surf. Sci. **107**, 459 (1981).

[4]R. Kutner, Phys. Lett. **81A**, 239 (1981).

[5]R. A. Tahir-Kheli (unpublished).

[6]T. Ala-Nissila, J. Kjoll, S. C. Ying, and R. A. Tahir-Kheli, preceding paper, Phys. Rev. B **44**, 2122 (1991).

[7]J. Kjoll, T. Ala-Nissila, and S. C. Ying, Surf. Sci. **218**, L476 (1989).

[8]M. Tringides and R. Gomer, Surf. Sci. **155**, 254 (1985).

[9]M. Tringides and R. Gomer, Surf. Sci. **166**, 419 (1986); **166**, 440 (1986).

[10]J. Kjoll, T. Ala-Nissila, and S. C. Ying (unpublished).

[11]R. A. Tahir-Kheli and R. J. Elliott, Phys. Rev. B **27**, 844 (1983).

[12]R. A. Tahir-Kheli, Phys. Rev. B **27**, 6072 (1983).

[13]R. A. Tahir-Kheli and N. El-Meshad, Phys. Rev. B **32**, 6166 (1985).

[14]P. C. W. Holdsworth and R. J. Elliott, Philos. Mag. A **54**, 601 (1986).

[15]R. A. Tahir-Kheli, P. C. Holdsworth, and R. J. Elliott (unpublished); R. A. Tahir-Kheli (unpublished).

[16]J. W. Chung, P. Estrup, and S. C. Ying, Phys. Rev. Lett. **56**, 749 (1986); D. Sahu, J. M. Kosterlitz, and S. C. Ying, in *The Structure of Surfaces II,* edited by J. F. Van der Veer and M. A. Van Hove (Springer-Verlag, New York, 1988).

[17]R. Gomer, Rep. Prog. Phys. **53**, 917 (1990).